Zn-doped PbO nanoparticles (NPs)/fluorine-doped tin oxide (FTO) as photoanode for enhancement of visible-near-infrared (NIR) broad spectral photocurrent application of narrow bandgap nanostructures: SnSe NPs as a case study

Majid Azarang, Mousa Aliahmad, A. Ghorban Shiravizadeh, H. R. Azimi, and Ramin Yousefi

---

Articles you may be interested in

Improvement of gas-sensing performance of ZnO nanorods by group-I elements doping
Journal of Applied Physics **122**, 224505 (2017); 10.1063/1.5009249

Zn-doped PbO nanoparticles (NPs)/fluorine-doped tin oxide (FTO) as photoanode for enhancement of visible-near-infrared (NIR) broad spectral photocurrent application of narrow bandgap nanostructures: SnSe NPs as a case study

Majid Azarang,[1] Mousa Aliahmad,[1] A. Ghorban Shiravizadeh,[2] H. R. Azimi,[3] and Ramin Yousefi[3,a)]

[1]*Department of Physics, University of Sistan and Baluchestan, 98135-674 Zahedan, Iran*
[2]*Department of Physics, Dezful Branch, Islamic Azad University (I.A.U.), Dezful, Iran*
[3]*Department of Physics, Masjed-Soleiman Branch, Islamic Azad University (I.A.U.), Masjed-Soleiman, Iran*

The capability of undoped and Zn-doped PbO nanoparticles (NPs) with different Zn concentrations, which were deposited on fluorine-doped tin oxide (FTO) glass, as a photoanode of the photocurrent device based on SnSe NPs, was investigated. An X-ray diffraction pattern of undoped PbO NPs indicated a mixture phase of orthorhombic, tetragonal phases of PbO, and a monoclinic phase of Pb_2O_3, while Zn-doped PbO NP samples showed a single orthorhombic phase of PbO, and these results were confirmed by Raman spectra results. Room temperature photoluminescence (PL) spectroscopy results of undoped and Zn(2%)-doped PbO NPs showed two emissions in the violet and red regions that belonged to the bandgap and defect, respectively. In addition, PL results indicated an extra emission for the Zn-doped PbO NPs in the green region by increasing Zn concentrations up to 4% and 6%. However, the red emission intensity was reduced by increasing Zn concentrations. Finally, undoped and Zn-doped PbO NPs with FTO glasses were used as photoanodes to measure the photocurrent response of SnSe NPs in the visible and near-infrared (NIR) regions, and the results were compared with FTO/TiO$_2$ as a photoanode, which has been typically used as photoanodes in quantum dot solar cells and dye-sensitized solar cells. It was observed that undoped and Zn-doped PbO NPs caused enhancement of photocurrent performance of the device. However, the responsivity of the device with FTO/Zn(2%)-doped PbO/ under NIR illumination source was higher than the responsivity of other devices under the same illumination source. *Published by AIP Publishing.* https://doi.org/10.1063/1.5050289

I. INTRODUCTION

Photocurrent devices, which operate in different regions such as ultraviolet (UV), visible, and near-infrared (NIR) regions, are important classes of optoelectronic devices that have different technological applications such as light-enhanced sensing, energy harvesting, light polarization analyzing, optical communication, flame detection, night vision cameras, missile approach warning systems, food industries, and medical applications.[1–13] In addition, visible-NIR broad spectral photocurrent applications are important for solar cell applications that are able to work at night or on cloudy days due to the presence of NIR waves in these conditions. Usually, narrow bandgap semiconductors such as Pb-, In-, and Sn-chalcogenide are the best candidates for fabrication of these photocurrents due to their unique properties such as big Bohr radius, easy bandgap engineering, stability, and their cost-effective synthesis process.[14–20] However, the main drawback of visible-NIR detectors is their low conversion gain in the NIR region. Therefore, it is very important to provide a method that can increase the efficiency of the photodetectors or solar cells in the NIR area while not distorting

the return on the visible area. Recently, an investigation on quantum dot solar cells (QDSCs) and dye-sensitized solar cells (DSSCs) that can operate at night and on cloudy days is one of the hot topics for research and they could revolutionize the solar cell industry.[21,22] In addition to layer absorption that has been used in these solar cells, the photoanode in these solar cells is the most important part due to the light that enters the cell from this part, and this part must be able to pass most of the solar spectrum. Fluorine-doped tin oxide (FTO) glass that was covered by TiO$_2$ paste is one of the common photoanodes in these solar cells due to the wide bandgap of these semiconductors and easy fabrication. Therefore, usually, researchers have tried to develop this common photoanode for the enhancement of solar cell performance.[23,24] Additionally, several other wide bandgap semiconductors such as ZnO,[25] ZnO/NiO composites,[26] ZnO/TiO$_2$ composites,[27] BiVO$_4$/rGO,[28] InAlN,[29] and MoS$_2$/rGO[30] have been deposited on FTO glass to fabricate different photoanodes. However, solar cell performance has been enhanced in these investigations but it cannot be seen as a significant effect of these photoanodes on enhancement of solar cell performance into the NIR region.

Among these wide bandgap semiconductors that have been used as photoanodes of QDSCs and DSSCs, PbO can also be used to fabricate photoanodes of these solar cells due

a)Author to whom correspondence should be addressed: Yousefi.ramin@gmail.com and raminyousefi@iaumis.ac.ir

to its wide bandgap that can be tuned from 1.9 to 3.5 eV by tuning its structure phase.[31] Lead oxide, like the other family of metal-oxides, has native point defects such as oxygen and lead vacancies.[32] Berashevich *et al.* reported a systematic study of the position of these point defects in the bandgap space of PbO.[33] They found that the O vacancies induce a very deep donor level close to the midgap of the bandgap space, which caused a red emission, while the Pb vacancies created a shallow defect level at just above the valence band, which acted as an acceptor and caused a green emission. Such defects in a semiconductor, which was used as a photoanode in a photodetector or solar cell, could enhance photon absorption by the solar cell and cause an increase in the efficiency of solar cells. In addition, a suitable doping element, which can play as a bandgap engineering factor in PbO and affect defect emissions such as O-vacancy emission, is able to increase the capability of photoanode performance. Zinc is one of these elements that can perform these missions very well due to unique properties of ZnO such as good absorption in the UV-visible region, which can increase the absorption coefficient of the solar spectrum in a solar cell.

In this work, photodetector devices were fabricated by different photoanodes such as FTO/TiO$_2$/, FTO/undoped PbO/, and FTO/Zn-doped PbO/ with different zinc concentrations. The absorption layer was SnSe nanoparticles (NPs) due to its small bandgap value, which is in the NIR region. In addition, according to our previous work, such NPs could be also absorbed in the visible spectrum due to its several defects that have energy levels in the visible region. Therefore, the fabrication devices will be photodetectors that work in the visible-NIR broad spectrum. The TiO$_2$ NPs were a commercial P-25 paste, while PbO and SnSe NPs were synthesized by a simple sol-gel and co-precipitation methods, respectively. As far as we can tell, there is no such study about the effects of PbO NPs on photoanode of photodetectors so far.

II. EXPERIMENT

A. Synthesis NPs and fabrication of photodetector devices

Undoped PbO NPs and SnSe NPs were synthesized similarly to our previous works.[31,34] Zn-doped PbO NPs were synthesized by different zinc concentrations (2%, 4%, and 6%). Different photodetector devices, which had different photoanodes such as FTO/TiO$_2$/, FTO/undoped PbO/, and FTO/Zn-doped PbO/ with different Zn concentrations, were fabricated according to our previous work that was used to fabricate photodetectors based on PbSe NPs.[20] A mixture of ethyl cellulose and alcohol was used to deposit NPs on FTO glasses. Au film with 10 nm thickness was sputtered on the FTO glasses by a sputter coater setup (DSR, Nanostructured Coatings Co., Iran), and these Au coated FTO glasses were used as counter electrodes in fabricated optical cell devices. A mixture of 0.5M of KI and 0.05M of I$_2$ was dissolved in ethylene glycol and this solution was used as the electrolyte. 0.25 cm^2 and 5 cm were applied as the illuminated area of the specimens and the distance between the films and the light source, respectively. A chopper was used for ON and OFF duration of the light

source for determination of the photocurrent behavior of the devices. Various light-emitting diodes (LEDs) such as the white LED and LEDs with wavelengths of 470 nm (blue LED), 560 nm (green LED), and 900 nm (NIR LED) were used as light sources for photocurrent measurements. The sensitivity of the samples was measured under 100 mW/cm^2 (1.5 Air mass) illumination from a homemade solar simulator, which included different LEDs with a broad spectrum from the ultraviolet (UV) region (320 nm) to the NIR region (1050 nm). Calibration of the light intensity was carried out by a standard silicon solar cell.

B. Characterizations

Crystal structures of the undoped and Zn-doped NPs were determined by an X-ray diffractometer (XRD, Philips, X'pert, system using Cu-K$_\alpha$ radiation) and a Raman spectrometer (Model: Almega ThermoNicolet Dispersive). The morphology of the samples was studied by transmission electron microscopy (TEM, Hitachi, H-7100) and field emission scanning electron microscopy (FESEM, TE-Scan MIRA3). Elemental mapping of the samples was obtained by FESEM. Optical properties of the products were investigated by a room temperature UV–Vis-NIR (Shimadzu UV-3600) and a photoluminescence spectrometer (UniRam PL spectrometer) with a He–Cd laser as a light source with a power of 200 mW and an excitation wavelength of 325 nm.

III. RESULTS AND DISCUSSION

The structure and phase of the undoped and Zn-doped PbO were indicated by XRD and Raman spectroscopy and these results are shown in Fig. 1. The XRD pattern of the undoped PbO indicates that this sample is included in a mixture of different phases such as the tetragonal (T-p) phase of PbO (Ref. code: 00-001-0796), orthorhombic (O-p) phase of PbO (Ref. code: 00-005-0570), and monoclinic (M-O) phase of Pb$_2$O$_3$ (Ref. code: 00-023-0331). However, the majority of the phases for this sample is the orthorhombic phase. This mixture of phases is also observed for the Zn(2%)-doped PbO in Fig. 1. On the other hand, increasing Zn concentration up to 4% causes a single phase that is the orthorhombic phase, and increasing Zn concentrations up to 6% cannot change the orthorhombic phase. The ionic radius of the substituted Zn^{2+} (0.74 Å) is smaller than that of Pb^{2+} (1.19 Å). Thus, Zn doping caused a slight shift in the XRD peaks toward higher diffraction angles by increasing the Zn concentration. This result provides indirect evidence that Zn^{2+} was incorporated into the crystal structure, causing the PbO crystal lattice to compress. In fact, such an effect of Zn-doping leads to the displacement of Pb ions, and these ions were placed in the orthorhombic phase.

Figure 1(b) shows Raman spectra of the undoped and Zn-doped PbO with different Zn concentrations. The Raman spectrum of the undoped PbO also indicates that this sample is included in a mixture of phases such as PbO that has peaks at 303 and 513 cm^{-1}, while a peak at 1031 cm^{-1} belongs to Pb$_3$O$_4$.[35] On the other hand, Zn-doped PbO samples show only the orthorhombic phase that has main peaks at 961 cm^{-1} and 1133 cm^{-1}.[36] Actually, the disorder
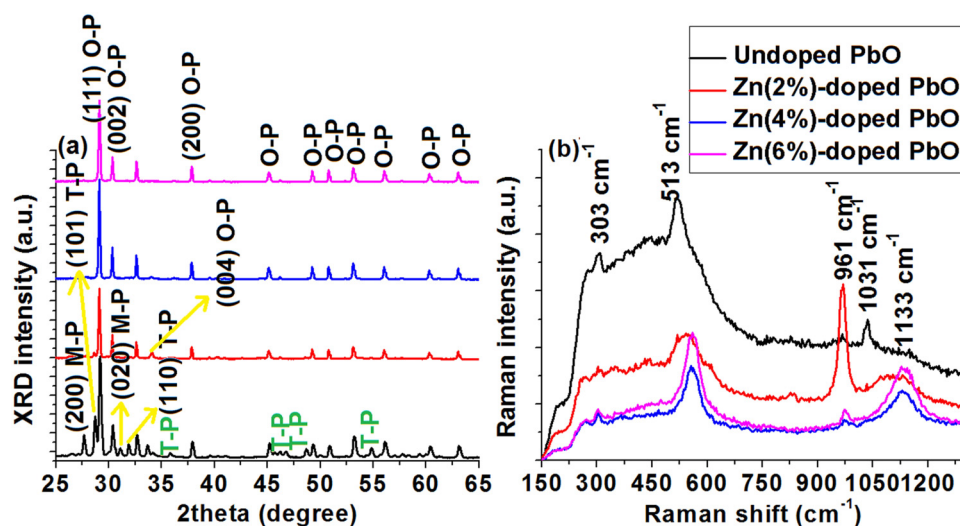
FIG. 1. (a) XRD patterns of the undoped PbO and Zn-doped PbO with different Zn concentrations. (b) Raman spectra of the undoped PbO NPs and Zn-doped PbO NPs with different Zn concentrations.

was caused by the substitution of lead with zinc and this is in good agreement with the XRD results.

Distribution of the elements in the Zn(4%)-doped PbO sample was investigated by elemental mapping. The results are shown in Fig. 2. According to these maps, the distribution of Zn-doping is uniform in this sample.

Optical properties of the undoped and Zn-doped PbO with different Zn concentrations were studied at room temperature; photoluminescence (PL) spectroscopy and the results are shown in Fig. 3. All of these spectra reveal two peaks, one a broad and strong peak at around 3 eV that belongs to the bandgap value of the PbO and the other a broad and weak peak at around 1.5 eV (red emission). However, deconvolution of the PL spectra of the Zn(4%)- and Zn(6%)-doped PbO shows a green emission peak for these samples. In addition, Zn-doping causes a widened bandgap of PbO. Green emission is due to O-vacancies in the PbO structure,[33] in which Zn-doping causes an increase in these O-vacancies that could be due to the change of phase structure from a mixture phase of PbO and Pb_3O_4 to a single phase of PbO. Furthermore, the red emission intensity and broadening are also changed by Zn-doping. The origin of the red emission is also oxygen interstitials,[37] which have been affected by Zn-doping because of different electronegativities of Zn and Pb as well as different ionic radii of these cations. As can be seen, the PL spectrum of the Zn(2%)-doped PbO shows higher and broader red emission. These different effects of Zn-doping on red emission could be due to the amount of Zn substitution in Pb ions in the PbO structure. In fact, increasing Zn-doping concentration may be because some Zn atoms cannot be substituted with Pb ions and this behavior affects O-interstitials and O-vacancies. The appearance of green emissions only in the samples with higher Zn-doping concentration could be evidence of our claim about this subject.

A TEM image of Zn(4%)-doped PbO and a FESEM image of SnSe NPs are shown in Figs. 4(a) and 4(b), respectively. In addition, the UV-Vis-NIR spectrum of the SnSe NPs can be seen, which shows an absorption edge around 1000 nm for SnSe NPs (the UV-Vis part of this spectrum is not shown here, because no absorption peak was observed), as shown in Fig. 4(c). A schematic of the fabricated photodetector device is shown in Fig. 4(d). This schematic reveals that the fabrication devices were illuminated under different LEDs, which were coupled with a chopper. Different photoanodes were used in this device such as $FTO/TiO_2/$, FTO/undoped PbO/, and FTO/Zn-doped PbO/ with different Zn concentrations.
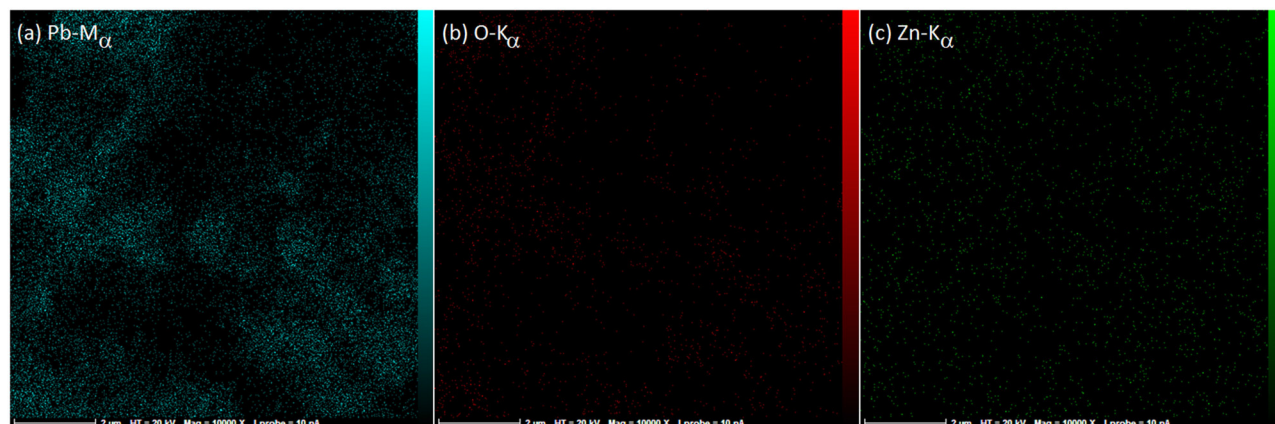

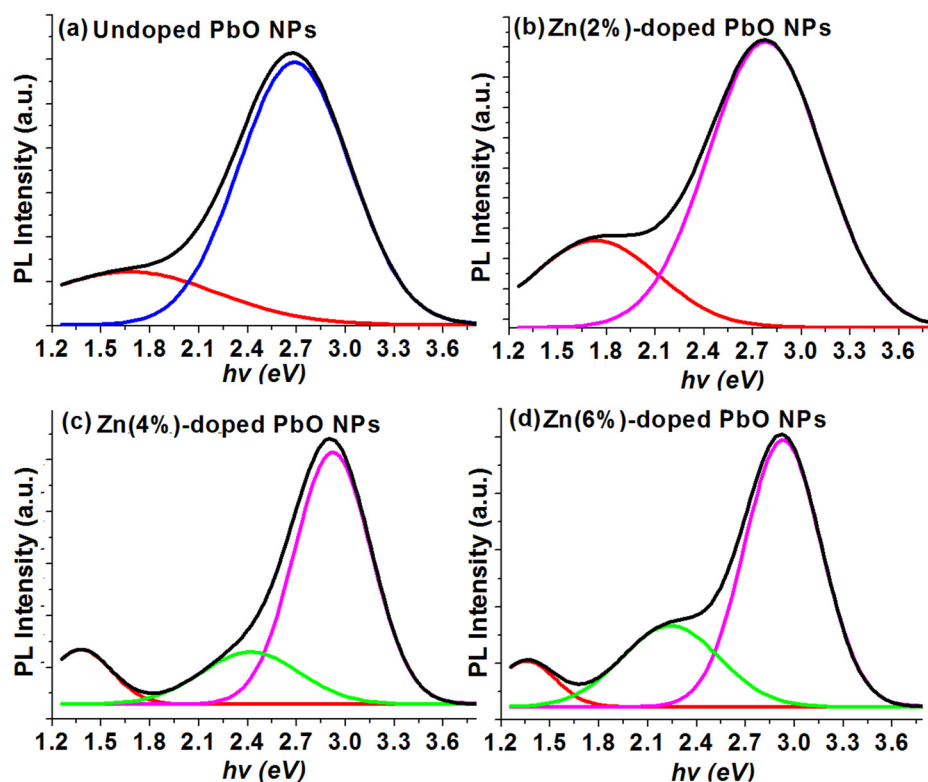FIG. 2. Elemental mapping of the elements in Zn(4%)-doped PbO.

FIG. 3. PL spectrum and its deconvolution peaks of (a) undoped PbO NPs, (b) Zn(2%)-doped PbO NPs, (c) Zn(4%)-doped PbO NPs, and (d) Zn(6%)-doped PbO NPs.

J-V measurements to obtain the resistance of the devices, which were fabricated by FTO/TiO$_2$/, FTO/undoped PbO/, and FTO/Zn(6%)-doped PbO/, were carried out under dark and white light source illuminations and the results are shown in Fig. 5(a). As can be seen, the resistance of the samples is approximately the same under dark conditions. On the other hand, a significant decreasing resistance of the devices that were fabricated by FTO/undoped PbO/ and
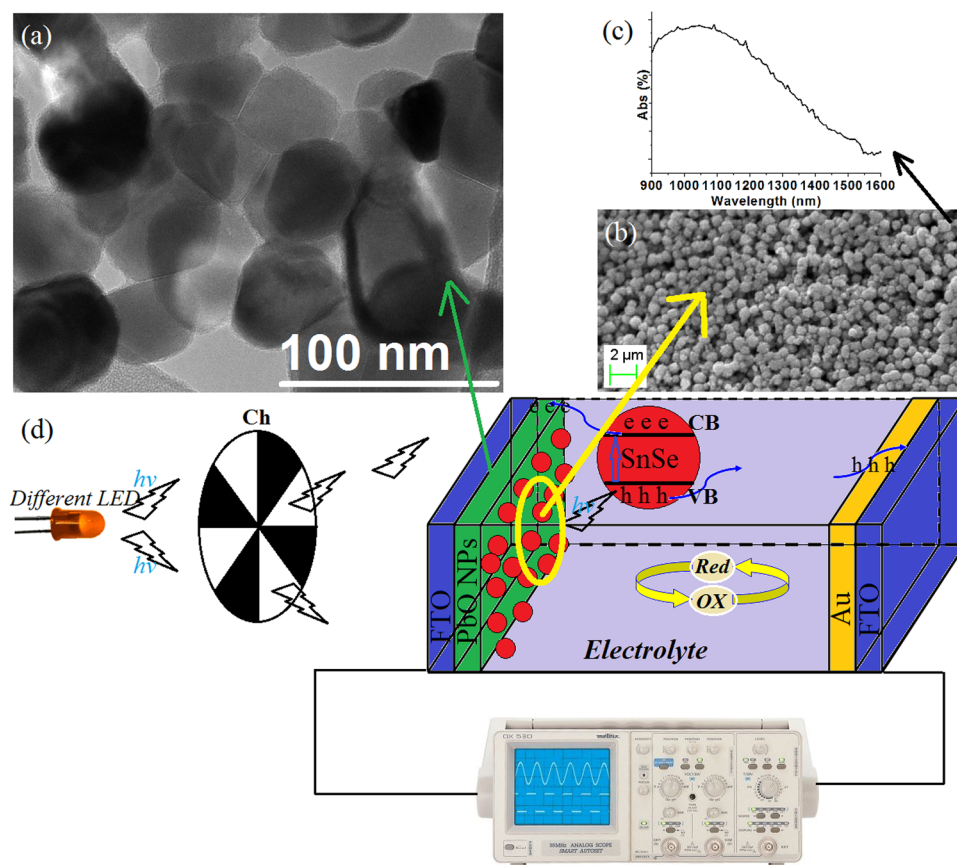

FIG. 4. (a) TEM image of the Zn(4%)-doped PbO. (b) SEM image of SnSe NPs. (c) UV-Vis-NIR spectrum of the SnSe NPs. (d) Schematic of fabricated device that was used to measure photocurrent intensity.
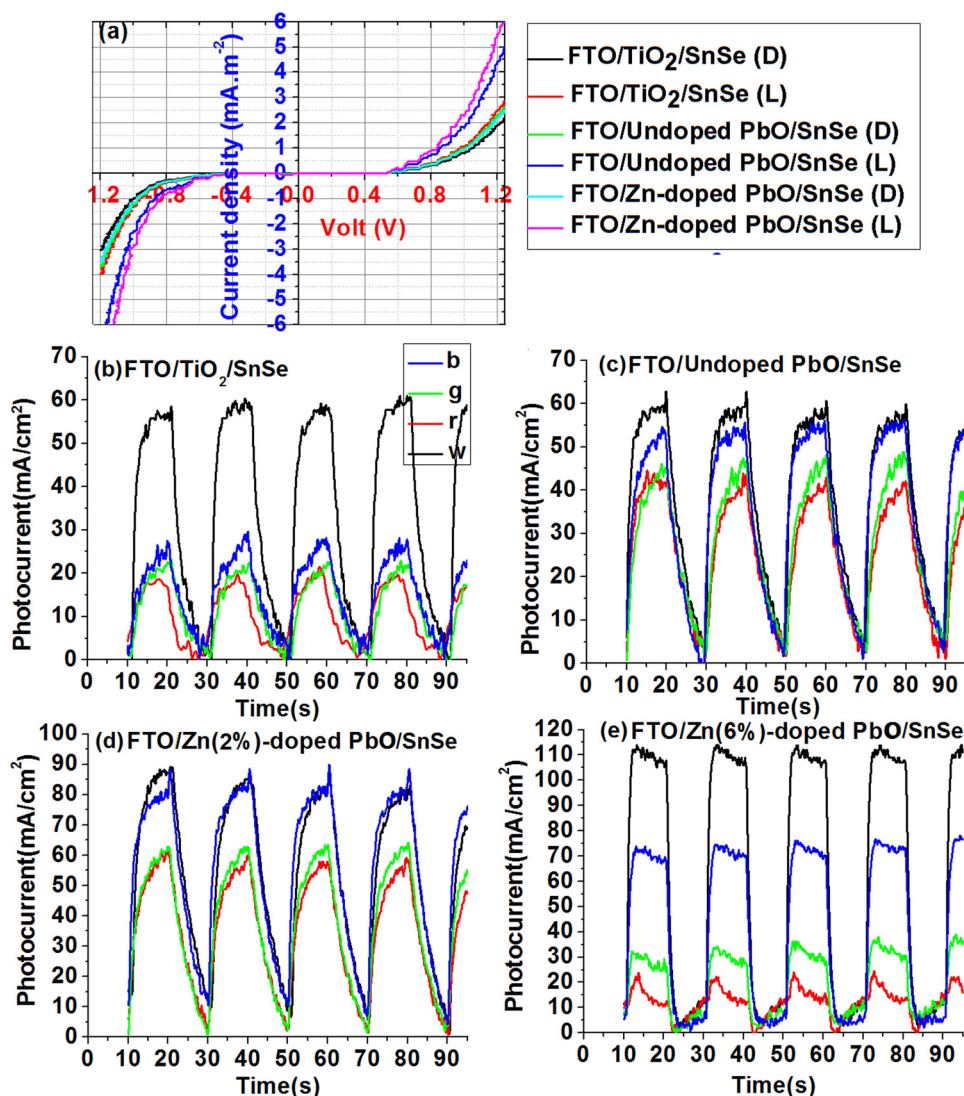
FIG. 5. (a) *J-V* curves of the photocurrent devices with different photoanodes under a white LED illumination. Photocurrent response of photocurrent devices with different photoanodes: (b) FTO/TiO$_2$/SnSe, (c) FTO/Undoped PbO/SnSe, (d) FTO/Zn(2%)-doped PbO/SnSe, and (e) FTO/Zn(6%)-doped PbO/SnSe under white (w), blue (b), green (g), and NIR (r) LED illumination.

FTO/Zn(6%)-doped PbO/ was observed in comparison to the resistance of the device that was fabricated by FTO/TiO$_2$/ under illumination conditions. In fact, these results indicate that optical properties of the photoanodes play a significant role to decrease the resistance of the photodetector device under light illumination conditions.

Photocurrent measurements under four different LEDs such as white (w), blue (b), green (g), and NIR (r) for different samples were carried out and the results are shown in Figs. 5(b)–5(e). It can be observed that the photocurrent intensity of the devices with FTO/TiO$_2$/ and FTO/undoped PbO/ photoanodes is the same approximately under chopper of white LED. On the other hand, the photocurrent intensity of the devices with FTO/Zn-doped PbO/ photoanodes under chopper of white LED is higher, and increasing the Zn-concentration leads to an increase in photocurrent. However, the photocurrent intensity changes under other LEDs are different. As can be seen, photocurrent intensity is higher for the devices, which were used in undoped and Zn-doped PbO NPs in their photoanodes, under chopper of blue, green, and NIR LEDs. In addition, the device with FTO/Zn(2%)-doped PbO/ as the photoanode shows the highest photocurrent intensity under colored LEDs. It could

be due to absorption of some of the NIR photons by the photoanode. If we look at the PL spectra, we can see that the ratio of I$_{NIR}$/I$_{UV}$ of the Zn(2%)-doped PbO NPs is bigger than the ratio of the other samples. On the other hand, this sample as a photoanode shows higher photocurrent under NIR illumination as compared with the other samples. In fact, this absorption can enhance photocurrent generation, which was generated by SnSe NPs, and caused an increase in photocurrent intensity in the NIR region. A similar phenomenon was observed by Wong *et al.* for DSSCs that had ZnO NPs as photoanodes. They observed that ZnO with higher defect emissions in orange-red regions showed higher effeminacy for the DSSCs.[38]

All of these different photocurrent performances could be dependent on the optical properties of undoped and Zn-doped PbO NPs. To show the effects of optical properties of photoanodes on the obtained results, TiO$_2$ NPs (P-25) were characterized by PL (the PL spectrum is not shown here) and a narrow and weak peak in the UV region was observed, while it showed a broad and strong peak in the visible regions from 480 nm to 700 nm. In fact, this PL did not show any red emission peak in the NIR region unlike the PbO NPs. Actually, a broader and stronger red emission in

TABLE I. τ_r and τ_f time of photocurrent devices under different illumination sources.

	LEDs		
	Blue LED (470 nm)	Green LED (560 nm)	NIR LED (900 nm)
Samples	τ_r (s)/τ_f (s)	τ_r (s)/τ_f (s)	τ_r (s)/τ_f (s)
FTO/TiO$_2$/	1.3/1.5	1.6/2.1	2.6/2.9
FTO/undoped PbO/	0.9/1.1	1.3/1.6	1.7/1.8
FTO/Zn-doped PbO/	0.6/0.8	0.7/0.9	0.6/0.9

the PL spectrum of the Zn(2%)-doped PbO NPs indicates that this sample has the higher trapping centers for the NIR photons. Therefore, such photoanodes can help SnSe NPs to convert NIR photons into current and lead to an increase in gain conversion of this device in the NIR region. In addition, rise (τ_r) and fall (τ_f) times of the photodetectors were compared and the results are shown in Table I. As can be seen, the FTO/Zn-doped PbO/ photoanode not only causes enhancement of photocurrent intensity of the photodetector but also leads to obtaining a faster photodetector in a broad spectrum. However, these times are slower than photosensors based on a single nanowire such as CdS, SnS, and SnSe NW.[39,40] Of course, it should be noted that the current work is a very simple and cost-effective method to fabricate a photosensor that works in the broad spectrum from the visible to the NIR regions, and it is the most important advantage of the current work. In addition, the higher photocurrent intensity of the FTO/Zn(6%)-doped PbO/ photoanode under white illumination could also be due to different PL spectrum features of Zn(6%)-doped PbO NPs in comparison to the other samples [Fig. 3(d)]. In fact, if we look at the PL spectrum of this sample [Fig. 3(d)], we can observe that this spectrum includes red, green, and violet emission, while the PL spectrum of the other samples [except Zn(4%)-doped PbO] shows only red and violet emissions. Therefore, defect levels are more in the Zn(6%)-doped sample in comparison to the other samples that are the most important factors to absorb photons from white light and cause an increase in the photocurrent intensity.
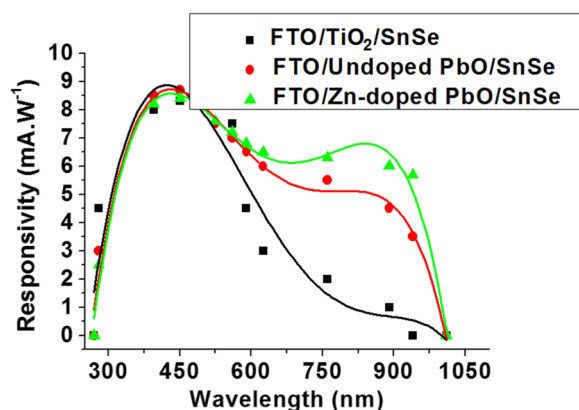

FIG. 6. Responsivity of the photocurrent devices that were obtained by illumination of the devices under a solar simulator with broad spectrum wavelength from 320 nm till 1050 nm.

An important figure-of-merit of a photodetector device is responsivity (R) that can be calculated by the following equation:

$$R = \frac{I_P}{P \times S}, \qquad (1)$$

where I_P is the generated photocurrent, P is the LED power, and S is the effective area, which is $0.25\,\text{cm}^2$ in the current work. This parameter was obtained from different devices by a solar simulator and the results are shown in Fig. 6. As can be seen, all devices show a good response to the visible part of the electromagnetic spectrum, while the response of the devices to the NIR sources of the simulator is different. In fact, the device that is included in the FTO/TiO$_2$ photoanode did not respond to the NIR, while we can see a good response to the NIR from the devices with PbO NPs in their photoanodes. In addition, this response is higher for the photoanode with Zn-doped PbO NPs. In fact, these results indicate that the photodetector device with the FTO/Zn(2%)-doped PbO NPs/ SnSe/(KI+I$_2$)/Au/FTO configuration is one of the best devices as a photodetector that can work in a broad spectrum from the visible to the NIR regions.

IV. CONCLUSION

A comparison study about the effects of undoped and Zn-doped PbO NPs with different Zn concentrations on the photoanode of photodetectors that were included in SnSe NPs as an absorption layer was conducted. XRD and Raman's results indicated that the undoped and Zn(2%)-doped PbO NPs were included in a mixture of phases that were tetragonal, orthorhombic, and monoclinic, while Zn(4-6%)-doped PbO NPs were included only in a single phase that was orthorhombic. PL results indicated two emissions in the UV and NIR regions for the undoped and Zn-doped PbO NPs as well as a green emission for the Zn(4-6%)-doped PbO NPs. Photodetectors that were fabricated by these photoanodes showed that FTO/Zn(2%)-doped PbO/ as a photoanode was the best candidate for the enhancement of photocurrent performance of SnSe NPs in a broad spectrum from the visible to the NIR region. In fact, it was concluded that Zn(2%)-doped PbO NPs had higher trapping centers in the NIR region. Therefore, this device showed higher photocurrent intensity in the NIR region compared to the other devices. Surely, such a configuration can be a good candidate for fabrication of QDSCs that can be worked at night or on cloudy days in the future.

[1]S. Khosravi Ghandomani, B. Khoshnevisan, and R. Yousefi, J. Mater. Sci.: Mater. Electron 1–8 (2018).

[2]B. Sun, M. P. Edgar, R. Bowman, L. E. Vittert, S. Welsh, A. Bowman, and M. J. Padgett, Science **340**, 844–847 (2013).

[3]T. Mueller, F. Xia, and P. Avouris, Nat. Photonics **4**, 297–301 (2010).

[4]H. Tan, G. Liu, X. Zhu, H. Yang, B. Chen, X. Chen, J. Shang, W. D. Lu, Y. Wu, and R. W. Li, Adv. Mater. **27**, 2797–2803 (2015).

[5]T. Ling, S. A. Kulinich, Z. L. Zhu, S. Z. Qiao, and X. W. Du, Adv. Funct. Mater. **24**, 707–715 (2014).

[6]J. D. Yao, J. M. Shao, S. W. Li, D. H. Bao, and G. W. Yang, Sci. Rep. **5**, 14184 (2015).

[7]Z. Xia, P. Li, Y. Wang, T. Song, Q. Zhang, and B. Sun, ACS Appl. Mater. Interfaces **7**, 24136–24141 (2015).

[8]L. Su, Y. Zhu, D. Yong, M. Chen, X. Ji, Y. Su, X. Gui, B. Pan, R. Xiang, and Z. Tang, ACS Appl. Mater. Interfaces **6**, 14152–14158 9 (2014).

[9]D. Shao, M. Yu, H. Sun, G. Xin, J. Lian, and S. Sawyer, ACS Appl. Mater. Interfaces **6**, 14690–14694 (2014).

[10]M. A. Baghchesara, M. Cheraghizade, F. Jamali-Sheini, and R. Yousefi, J. Mater. Sci.: Mater. Electron. **28**, 4475 (2017).

[11]V. Fernández-Ibañez, A. Soldado, A. Martínez-Fernández, and B. dela Roza-Delgado, Food Chem. **113**, 629–634 (2009).

[12]C. Harbeck, R. Faurie, and T. Scheper, Anal. Chim. Acta **501**, 249–253 (2004).

[13]Z. Guo, S. Park, J. Yoon, and I. Shin, Chem. Soc. Rev. **43**, 16–29 (2014).

[14]M. Cheraghizade, R. Yousefi, F. Jamali-Sheini, M. R. Mahmoudian, A. Sa'aedi, and N. M. Huang, Mater. Sci. Semicond. Process. **26**, 704–709 (2014).

[15]M. A. Baghchesara, R. Yousefi, M. Cheraghizade, F. Jamali-Sheini, A. Sa'aedi, and M. R. Mahmoudian, Mater. Res. Bull. **77**, 131–137 (2016).

[16]R. Yousefi, M. R. Mahmoudian, A. Sa'aedi, M. Cheraghizade, F. Jamali-Sheini, and M. Azarang, Ceram. Int. **42**, 15209–15216 (2016).

[17]M. Cheraghizad, F. Jamali-Sheini, and R. Yousefi, Appl. Phys. A **123**, 390 (2017).

[18]Jiandong Yao, Zhaoqiang Zheng, and Guowei Yang, Adv. Funct. Mater. **27**, 1701823 (2017).

[19]Jiandong Yao, Zexiang Deng, Zhaoqiang Zheng, and Guowei Yang, ACS Appl. Mater. Interfaces **8**, 20872–20879 (2016).

[20]A. Ghorban Shiravizadeh, S. M. Elahi, S. A. Sebt, and R. Yousefi, J. Appl. Phys. **123**, 083102 (2018).

[21]N. Robertson, Angew. Chem. Int. Ed. **47**, 1012–1014 (2008).

[22]J. Duan, Y. Duan, Y. Zhao, Y. Wang, Q. Tang, and B. He, J. Energy Chem. **27**, 742–747 (2018).

[23]A. Trenczek-Zajac, Mater. Sci. Semicond. Process. **83**, 159–170 (2018).

[24]D. S. U. Peiris, P. Ekanayake, and M. Iskandar Petra, Org. Electron. **59**, 399–405 (2018).

[25]P. R. Nikam, P. K. Baviskar, S. Majumder, J. V. Sali, and B. R. Sankapal, J. Colloid Interface Sci. **524**, 148–155 (2018).

[26]X. Zhou, J. Yang, J. Cheng, Y. Qiang, H. Shi, and Y. Xie, J. Alloys Compd. **765**, 287–298 (2018).

[27]A. Kumar Chandiran, M. Abdi-Jalebi, M. K. Nazeeruddin, and M. Grätzel, ACS Nano **8**, 2261–2268 (2014).

[28]T. Soltani, A. Tayyebi, and B.-Kyu Lee, Sol. Energy Mater. Sol. Cells **185**, 325–332 (2018).

[29]M. Alizadeh, G. Boon Tong, M. S. Mehmood, K. W. Qader, S. A. Rahman, and B. Shokri, Sol. Energy Mater. Sol. Cells **185**, 445–455 (2018).

[30]M. Shang, H. Qi, C. Du, H. Huang, S. Wu, J. Zhang, and W. Song, Sens. Actuators B **266**, 71–79 (2018).

[31]R. Yousefi, A. Khorsand Zak, F. Jamali-Sheini, N. M. Huang, W. J. Basirun, and M. Sookhakian, Ceram. Int. **40**, 11699–11703 (2014).

[32]S. Aggarwal and R. Ramesh, Annu. Rev. Mater. Sci. **28**, 463–499 (1998).

[33]J. Berashevich, O. Semeniuk, O. Rubel, J. A. Rowlands, and A. Reznik, J. Phys. Condens. Matter **25**, 075803 (2013).

[34]A. Ghorban Shiravizadeh, R. Yousefi, S. M. Elahi, and S. A. Sebt, Phys. Chem. Chem. Phys. **19**, 18089–18098 (2017).

[35]L. Burgio, R. J. H. Clark, and S. Firth, Analyst **126**, 222–227 (2001).

[36]M. Cortez-Valadez, A. Vargas-Ortiz, L. Rojas-Blanco, H. Arizpe-Chávez, M. Flores-Acosta, and R. Ramírez-Bon, Physica E **53**, 146–149 (2013).

[37]A. Aliakbari, E. Najafi, M. M. Amini, and S. W. Ng, Monatsh. Chem. **145**, 1277–1285 (2014).

[38]K. K. Wong, A. Ng, X. Y. Chen, Y. H. Ng, Y. H. Leung, K. H. Ho, A. B. Djurišić, A. M. C. Ng, W. K. Chan, L. Yu, and D. L. Phillips, ACS Appl. Mater. Interfaces **4**, 1254–1261 (2012).

[39]D. Zheng, H. Fang, P. Wang, W. Luo, F. Gong, J. C. Ho, X. Chen, W. Lu, L. Liao, J. Wang, and W. Hu, Adv. Funct. Mater. **26**, 7690–7696 (2016).

[40]D. Zheng, H. Fang, P. Wang, M. Long, F. Wu, P. Wang, F. Gong, X. Wu, J. C. Ho, and W. Hu, ACS Nano **12**, 7239–7245 (2018).